

Electronic supplementary information

NiS gradient distribution on arrayed porous carbonized grapefruit peel for water splitting

Xiaoyun Zhang,^a Shifan Zhu,^a Lili Song,^a Yixue Xu,^a Yuqiao Wang^{*a}

^a Research Center for Nano Photoelectrochemistry and Devices, School of Chemistry and Chemical Engineering, Southeast University, Nanjing, 211189, China

*Corresponding author. E-mail address: yqwang@seu.edu.cn (Y. Wang)

Content includes: Experimental section, figures and tables.

1 Experimental section

2 Figures and tables

Fig. S1 The synthesis process of NiS/APC.

Fig. S2 SEM images and corresponding EDX elemental mappings of (a) grapefruit peel and (b) carbonized grapefruit peel.

Fig. S3 (a-c) SEM image and (d) corresponding EDX elemental mappings of M-NiS/APC.

Fig. S4 EDX elemental mappings of (a) H-NiS/APC and (b) L-NiS/APC.

Fig. S5 EDS element content of NiS/APC.

Fig. S6 XPS survey spectrum of M-NiS/APC.

Fig. S7 The theoretical models of (a) H-NiS/APC, (b) M-NiS/APC and (c) L-NiS/APC.

Fig. S8 Charge density difference diagrams and corresponding electron localization function of H-NiS/APC.

Fig. S9 The adsorption model of the (a) L-NiS/APC and (b) H-NiS/APC for OER. The adsorption model of the (c) L-NiS/APC and (d) H-NiS/APC for HER.

Fig. S10 (a) The N₂ isothermal absorption/desorption curves and (b) pore size distribution curves of NiS/APC. (c) Nyquist plots of NiS/APC under 0.4 V potential. (d) Relationship between Z' and $\omega^{-1/2}$ in the low-frequency region calculated from EIS measurement results.

Fig. S11 The chronoamperometric stability of M-NiS/APC for (a) HER and (b) OER for 12 h at current density of 10 mA/cm². The inset images are LSV curves of M-NiS/APC before and after chronoamperometric stability test for HER and OER, respectively.

Fig. S12 CV curves with different scan rate in the 0.11-0.21 V vs. RHE region of NiS/APC.

Fig. S13 Gas collector for a two-electrode water splitting configuration. H₂ and O₂ produced at 0, 10, 20, 30, 40, 50 and 60 min.

Table S1 Actual mass ratios of NiS/APC obtained from ICP.

Table S2 XPS results of NiS/APC.

Table S3 Textural parameters of NiS/APC obtained from N₂ adsorption measurement.

Table S4 Electrical equivalent circuit parameters obtained by fitting EIS results for HER.

Table S5 Electrical equivalent circuit parameters obtained by fitting EIS results for OER.

Table S6 Comparison of electrocatalytic performance of M-NiS/APC and NiS-based OER electrocatalysts.

Table S7 Comparison of HER performance of M-NiS/APC with previously reported HER electrocatalysts.

Table S8 Comparison of OER performance of M-NiS/APC with previously reported OER electrocatalysts.

Table S9 Comparison of overall water splitting performance of M-NiS/APC with previously reported electrocatalysts.

Experimental section

Chemicals

High S element content grapefruit peel was collected in daily life. Grapefruit peel was washed with deionized water and passed through a 80-mesh sieve, following by drying in a vacuum oven at 80 °C for 24 h. Nickel nitrate hexahydrate ($\text{Ni}(\text{NO}_3)_2 \cdot 6\text{H}_2\text{O}$), ammonium fluoride (NH_4F), potassium hydroxide (NaOH) were purchased from Sinopharm Chemical Reagent Co., Ltd. Pt/C, RuO_2 and Nafion (5 wt%) were obtained from Sigma-Aldrich Chemical Reagent Co., Ltd. All reagents were of analytical grade and used without purification.

Synthesis of NiS/APC

1.0 g grapefruit peel and 1.0 g KOH were mixed through grinding. The mixture was transfer into porcelain boat and placed a tubular furnace with a 5 °C/min ramp rate in N_2 gas flow. Array porous carbon (APC) was obtained after 700 °C carbonization followed by washing, filtration and drying. 1.0 g APC and n g $\text{Ni}(\text{NO}_3)_2 \cdot 6\text{H}_2\text{O}$ (n = 1, 2 and 3) were added into 40 mL deionized water and stirred for 1 h. After dried at 80 °C, the mixture was carbonization under 500 °C with a heating rate of 5 °C/min in N_2 atmosphere. The obtained samples were donated as H-NiS/APC, M-NiS/APC and L-NiS/APC according to 1, 2 and 3 g $\text{Ni}(\text{NO}_3)_2 \cdot 6\text{H}_2\text{O}$ doses, respectively.

Materials characterization

Scanning electron microscopy (SEM, FEI Quanta 250) and energy dispersive X-ray spectroscopy were carried out to observe the morphologies and microstructures of samples. Transmission electron microscopy (TEM) was performed on a FEI Talos microscopy with a 200 kV accelerating voltage. X-ray diffraction (XRD, Shimazu XD-3A) was carried out to analyze the crystalline phase. X-ray photoelectron spectroscopy (XPS, Kratos AXIS ULTRA) was recorded to investigate the valance state of samples. N_2 sorption isotherms and pore distribution were recorded on a PS1-0530

instrument.

DFT calculations

First-principles calculations were performed using CASTEP package code based on DFT. The generalized gradient approximation (GGA) with Perdew-Burke-Ernzerhof (PBE) was used to describe the exchange-correlation interactions. The $3 \times 1 \times 1$ Monkhorst-Pack grids were applied for the DFT calculations. The electronic energy and forces were converged to within 10^{-4} eV and 0.05 eV/Å, respectively. The cutoff energy was set to 450 eV for the plane wave basis. The vacuum separation was larger than 15 Å to avoid interplanar interactions.

The Gibbs free energy of hydrogen evolution reaction (HER) and oxygen evolution reaction (OER) process was evaluated by following equation:

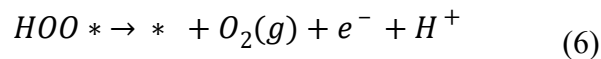
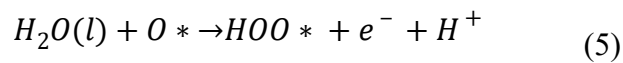
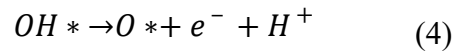
$$\Delta G_{H^*} = \Delta E_{H^*} + \Delta ZPE - T\Delta S \quad (1)$$

where ΔE_{H^*} was the change of total energy, ΔZPE is the zero-point energy change, and ΔS is the entropy change.

For HER, the samples were tested in alkaline conditions with potentials close to zero (vs. RHE), ΔG_{H^*} for HER can be calculated by the equation (2):

$$\Delta G_{H^*} = \Delta E_{H^*} + 0.24 \quad (2)$$

The four-electron pathway for OER can be summarized as follows:



where * represented the metal site on the surface, OH*, O* and HOO* represented the adsorption intermediates for OER.

The energy barrier (ΔG) of each step can be calculated through following equations:

$$\Delta G_O = G(O^*) - G(^*) - G(H_2O) + G(H_2) \quad (7)$$

$$\Delta G_{OH} = G(OH^*) - G(^*) - G(H_2O) + 1/2G(H_2) \quad (8)$$

$$\Delta G_{OOH} = G(OOH^*) - G(^*) - 2G(H_2O) + 3/2G(H_2) \quad (9)$$

Computational modeling

A three-dimensional model was used to simulate the electrolyte mass transfer in the COMSOL MULTIPHYSICS[®] software. To set the boundary conditions, the surface of electrode was assumed to contact with electrolyte ($x = 0$). The maximum value for KOH concentration was set to 1.0 M. The model was constructed with parameters of $10 \times 10 \times 10$ nm and the pore diameter was 2 nm according to the N₂ adsorption and desorption curves.

Electrochemical measurements

Electrochemical measurements were carried out on CHI 760E workstation in 1 M KOH aqueous solution. The HER and OER measurements were recorded in a three-electrodes cell, in which a glassy carbon electrode coated with NiS/APC acted as working electrode, a graphite rod and a saturated calomel electrode (SCE) were used as counter and reference electrodes, respectively. 1.0 mg NiS/APC, 0.2 mg acetylene black and 50 μ L Nafion were dispersed in 1.0 mL ethanol solution. 20 μ L electrocatalysts suspension were dropped onto the 3 mm diameter glassy carbon electrode with a mass loading is 0.28 mg cm⁻². The potentials versus reversible hydrogen electrode (RHE) were calculated by the equation: $E_{RHE} = E_{SCE} + 0.059 \times pH + 0.241$. Linear sweep voltammetry (LSV) curves were recorded at a scan rate of 2 mV/s with 90% iR-correction. Electrochemical impedance spectroscopy (EIS) was performed from 0.1 Hz to 100 kHz. Cyclic voltammetry (CV) curves were carried out at various scan rates (10 - 140 mV/s) to calculate double layer capacitance (C_{dl}) and corresponding electrochemical surface area (ECSA). Long-term stability was assessed by chronopotentiometry measurement. A two-electrode cell was constructed by both M-NiS/APC loaded nickel foam (1 cm \times 1 cm) to measure the overall water splitting performance. Faradaic efficiency

for overall water splitting was estimated based on the generated gas volume versus the theoretically calculated value for 60 min.

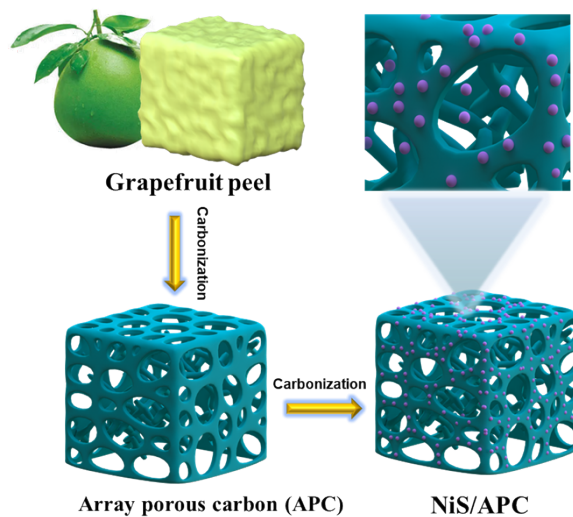


Fig. S1 The synthesis process of NiS/APC.

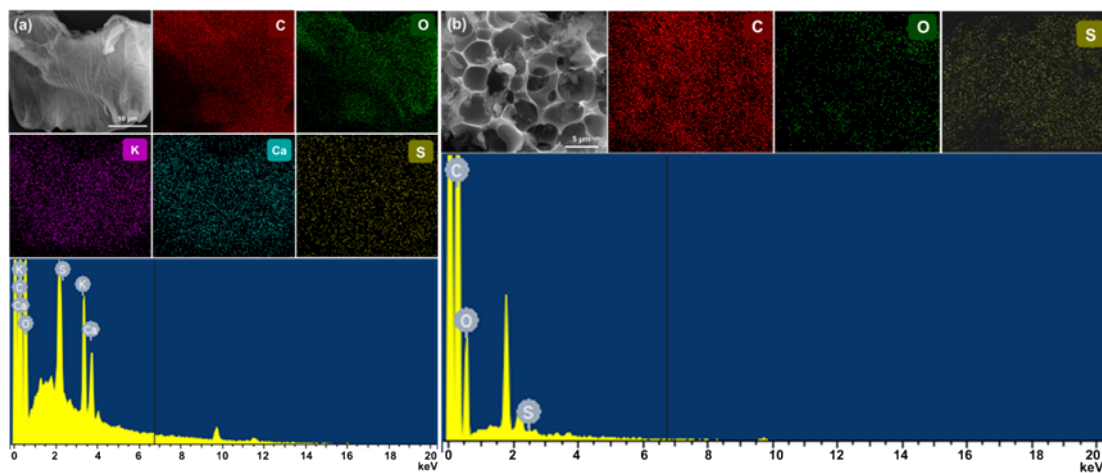


Fig. S2 SEM images and corresponding EDX elemental mappings of (a) grapefruit peel and (b) carbonized grapefruit peel.

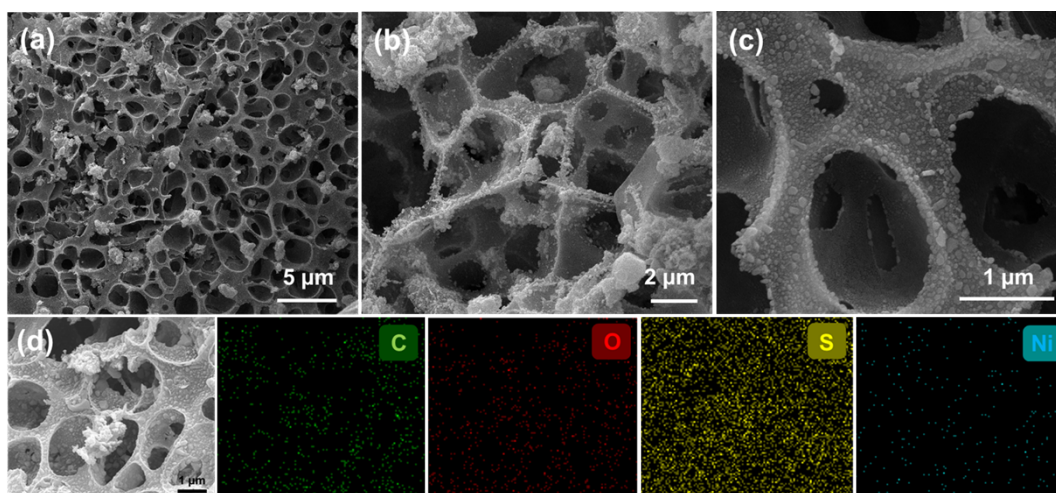


Fig. S3 (a-c) SEM image and (d) corresponding EDX elemental mappings of M-NiS/APC.

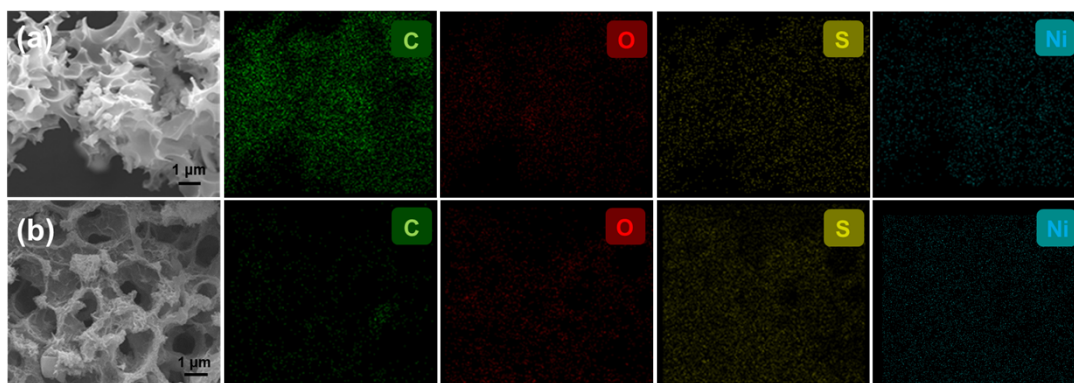


Fig. S4 EDX elemental mappings of (a) H-NiS/APC and (b) L-NiS/APC.

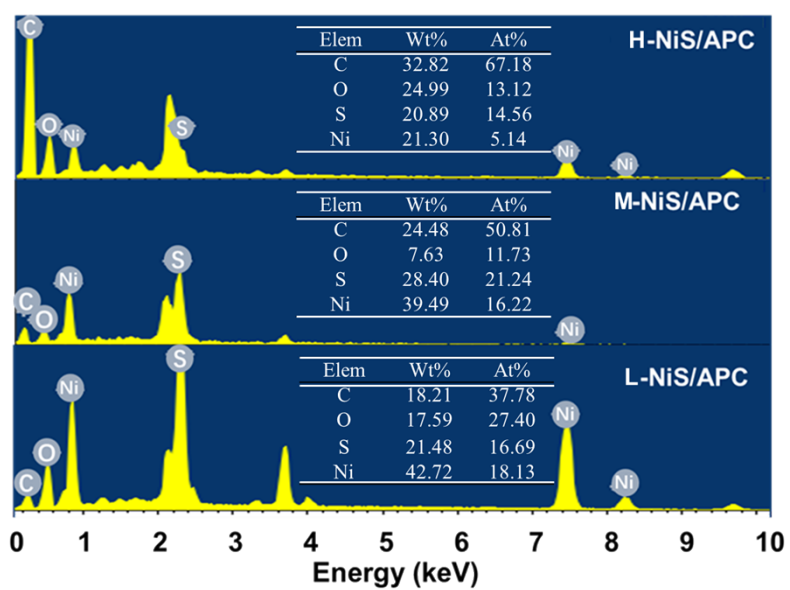


Fig. S5 EDS element content of NiS/APC.

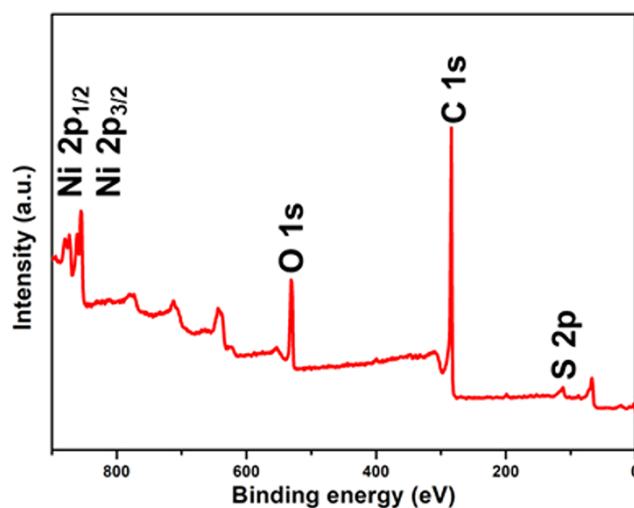


Fig. S6 XPS survey spectrum of M-NiS/APC.

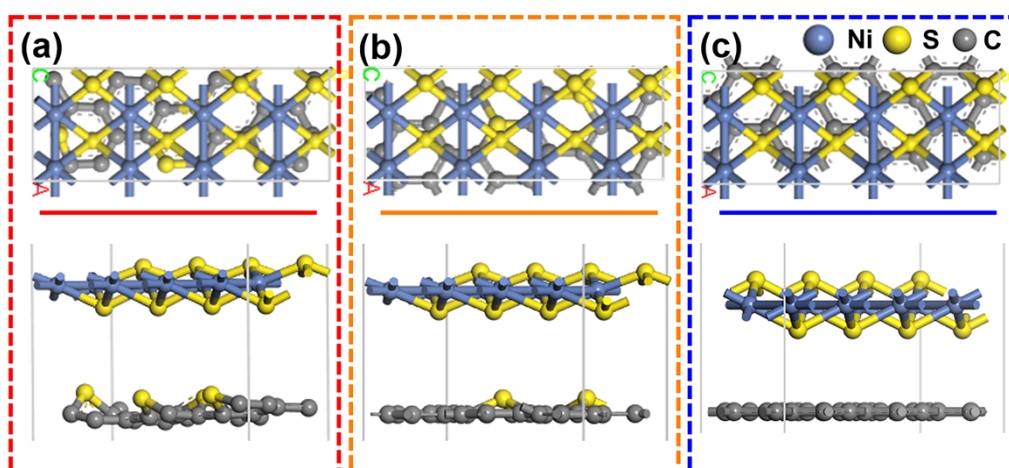


Fig. S7 The theoretical models of (a) H-NiS/APC, (b) M-NiS/APC and (c) L-NiS/APC.

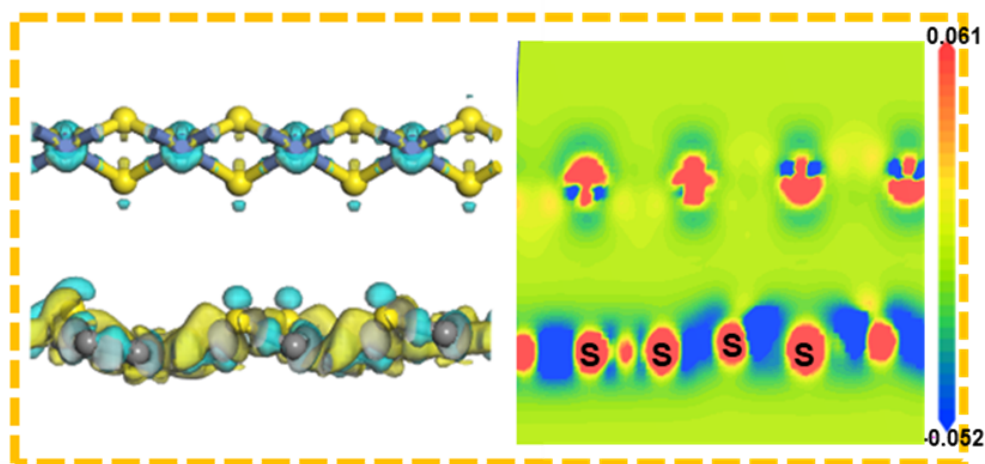


Fig. S8 Charge density difference diagrams and corresponding electron localization function of H-NiS/APC.

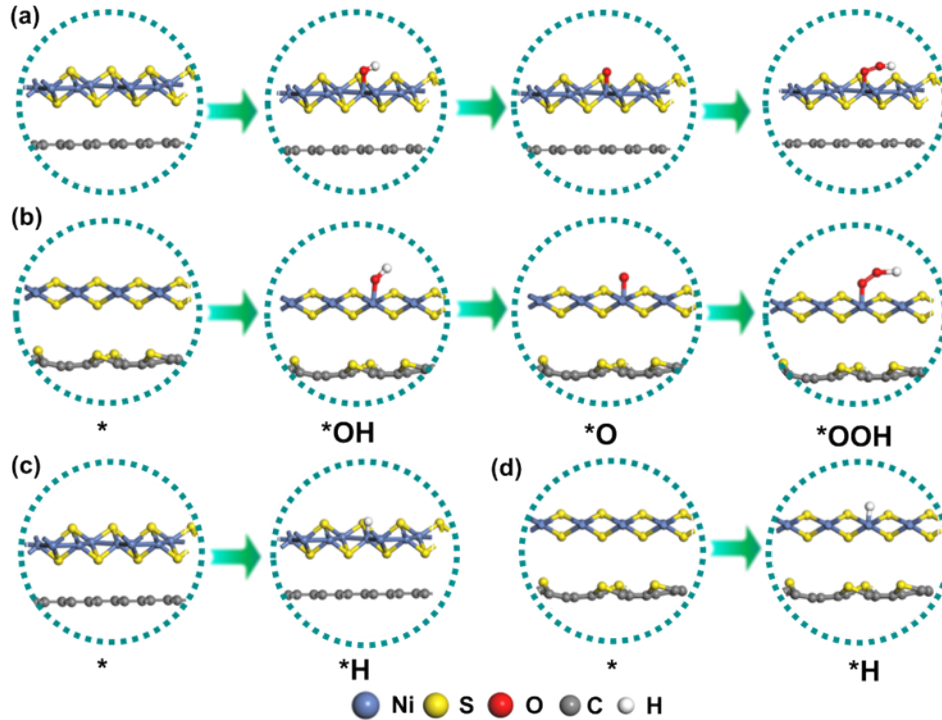


Fig. S9 The adsorption model of the (a) L-NiS/APC and (b) H-NiS/APC for OER. The adsorption model of the (c) L-NiS/APC and (d) H-NiS/APC for HER.

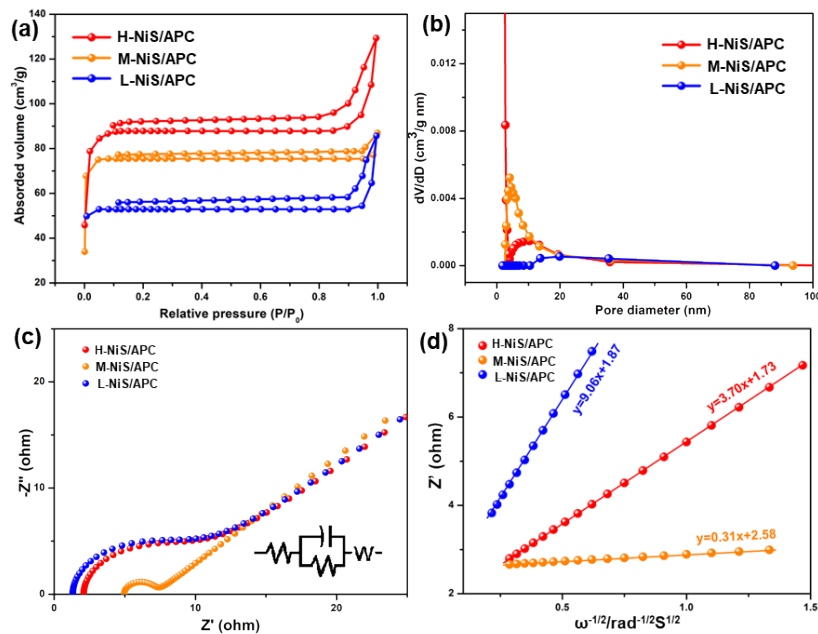


Fig. S10 (a) The N_2 isothermal absorption/desorption curves and (b) pore size distribution curves of NiS/APC. (c) Nyquist plots of NiS/APC under 0.4 V potential. (d) Relationship between Z' and $\omega^{-1/2}$ in the low-frequency region calculated from EIS measurement results.

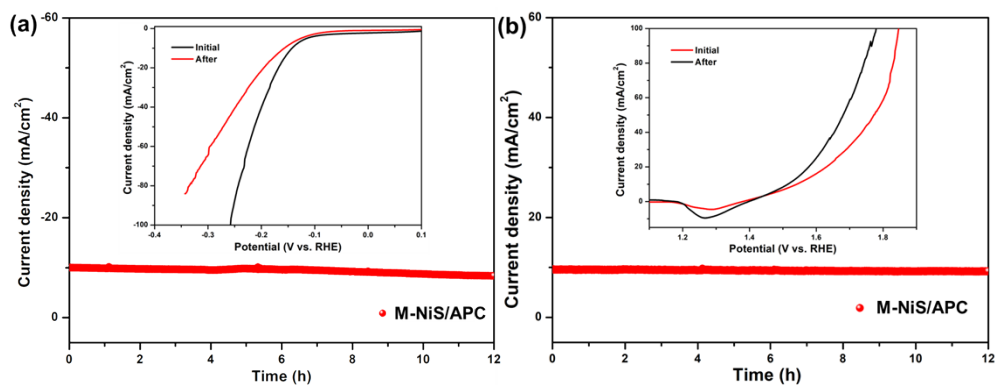


Fig. S11 The chronoamperometric stability of M-NiS/APC for (a) HER and (b) OER for 12 h at current density of 10 mA/cm^2 . The inset images are LSV curves of M-NiS/APC before and after chronoamperometric stability test for HER and OER, respectively.

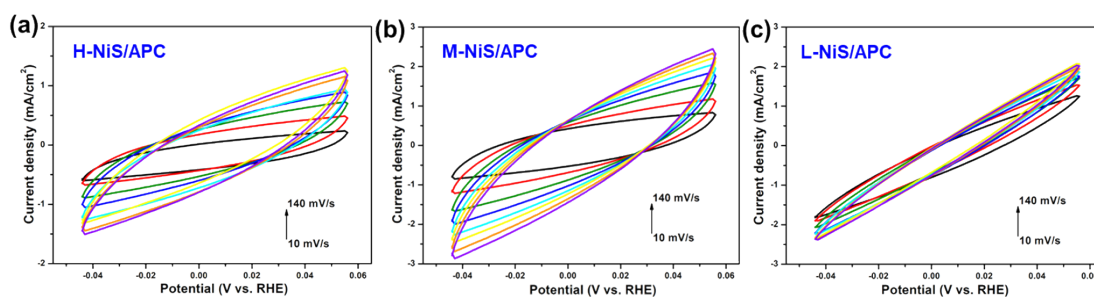


Fig. S12 CV curves with different scan rate in the 0.11 - 0.21 V vs. RHE region of NiS/APC.

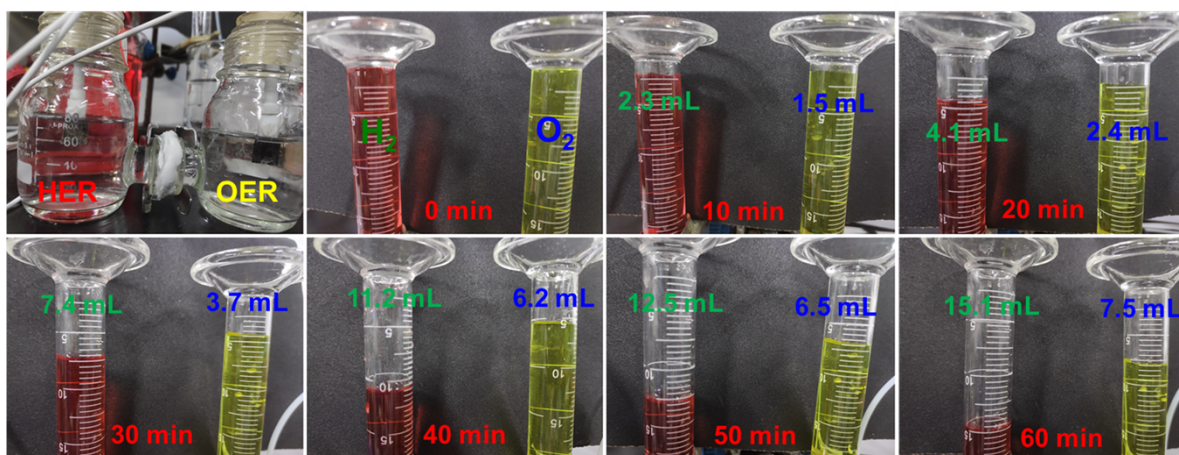


Fig. S13 Gas collector for a two-electrode water splitting configuration. H_2 and O_2 produced at 0, 10, 20, 30, 40, 50 and 60 min.

Table S1. Actual mass ratios of NiS/APC obtained from ICP-MS.

Sample	Mass ratio (Ni, wt%)
H-NiS/APC	17.94%
M-NiS/APC	38.08%
L-NiS/APC	24.32%

Table S2. XPS results of NiS/APC.

Elements	H-NiS/APC	M-NiS/APC	L-NiS/APC	Assignment
	Component (eV)/ Content (at, %)	Component (eV)/ Content (at, %)	Component (eV)/ Content (at, %)	
C 1s	283.8/55.6%	284.0/59.0%	283.9/55.5%	C-C/C=C
	284.6/29.6%	285.2/25.6%	284.6/35.0%	C-S
	288.2/14.8%	288.7/15.4%	288.1/9.5%	C=O
	854.6/17.8%	854.6/19.6%	853.8/20.4%	+2
	855.9/22.0%	855.9/15.7%	855.5/18.9%	+3
Ni 2p	860.9/24.0%	861.3/23.5%	860.7/21.4%	Sat.
	872.8/12.5%	872.9/13.7%	872.4/14.2%	+2
	875.8/4.8%	875.8/9.8%	875.1/11.0%	+3
	879.8/18.9%	879.7/17.7%	879.8/14.1%	Sat.
S 2p	163.2/35.4%	162.9/17.2%	162.9/25.2%	S-Ni (S 2p _{3/2})
	163.8/12.3%	163.9/26.2%	163.7/20.1%	S-Ni (S 2p _{1/2})
	164.4/18.5%	164.8/17.6%	164.3/16.8%	C-S-C
	168.2/33.8%	168.9/39.0%	168.5/37.9%	S-O

Table S3. Textural parameters of NiS/APC obtained from N₂ adsorption measurement.

Sample	S _{BET} (m ² g ⁻¹)	V _{total} (cm ³ g ⁻¹)	D (nm)
H-NiS/APC	557.1	0.34	2.45
M-NiS/APC	328.4	0.12	2.22
L-NiS/APC	157.4	0.12	3.09

Table S4. Active mass density of NiS/APC.

Samples	S _{BET} (m ² /g)	Mass ratio (wt%)	Active density (g/m ²)
H-NiS/APC	557.1	19.74	0.035
M-NiS/APC	328.4	38.08	0.169
L-NiS/APC	157.4	24.32	0.154

Note: The mass ratio of Ni was measured by ICP-MS.

Table S5. Electrical equivalent circuit parameters obtained by fitting EIS results for HER.

Electrocatalyst	R_s ($\Omega \text{ cm}^2$)	R_{ct} ($\Omega \text{ cm}^2$)
H-NiS/APC	2.43	56.62
M-NiS/APC	1.30	8.34
L-NiS/APC	2.29	23.14

Table S6. Electrical equivalent circuit parameters obtained by fitting EIS results for OER.

Electrocatalyst	R_s ($\Omega \text{ cm}^2$)	R_{ct} ($\Omega \text{ cm}^2$)
H-NiS/APC	2.59	34.30
M-NiS/APC	1.44	6.01
L-NiS/APC	3.17	14.30

Table S7. Comparison of electrocatalytic performance of M-NiS/APC and NiS-based OER electrocatalysts.

Electrocatalyst	Overpotential (mV) at 10 mA/cm ²	Tafel slope (mV/dec)	References
NiS/APC	286	69	This work
Fe-NiS ₂ /MoS ₂	280	92	<i>J. Mater. Chem. A</i> 2020 , 8, 17527-17536
Ni ₃ S ₂ @Ni ₃ B/NP	288	87	<i>Nanoscale</i> 2021 , 13, 17953-17960
V-NiPS ₃	290	78	<i>ChemSusChem</i> 2021 , 14, 2576-2584
Ni ₃ S ₂ /NF	303	111	<i>Appl. Catal. B Environ.</i> 2022 , 304, 120935
Fe ₃ O ₄ /NiS@CC	310	82	<i>J. Mater. Sci. Technol.</i> 2020 , 59, 92-99
MoS _x @Co ₉ S ₈ @Ni ₃ S ₂ /NF	310	107	<i>Langmuir</i> 2022 , 38, 3469-3479
NiS/NF	320	71	<i>ACS Sustainable Chem.</i> <i>Eng.</i> 2017 , 5, 7203-7210
Meso C-NiFeS	350	93	<i>ACS Appl. Energy Mater.</i> 2019 , 2, 5363-5372
NiS ₂ /MoS ₂ -CC	362	104	<i>Electrochimica Acta</i> 2019 , 326, 134983

Table S8. Comparison of HER performance of M-NiS/APC with previously reported HER electrocatalysts.

Catalyst	Electrolyte	Overpotential at 10 mA/cm ²	References
NiS/APC	1.0 M KOH	142 mV	This work
CoP@NCHNCs	1.0 M KOH	93 mV	[1]
U-Fe-β-Ni(OH) ₂ /NF	1.0 M KOH	121 mV	[2]
CdS@Ni ₃ S ₂ /Ni ₃ P	1.0 M KOH	130 mV	[3]
CoP-NC@NFP	1.0 M KOH	162 mV	[4]
Fe ₃ C-Co/NC	0.5 M H ₂ SO ₄	238 mV	[5]
Ni-Ni ₃ C-NCNT	1.0 M PBS	370 mV	[6]

Table S9. Comparison of OER performance of M-NiS/APC with previously reported OER electrocatalysts.

Catalyst	Electrolyte	Overpotential at 10 mA/cm ²	References
NiS/APC	1.0 M KOH	286 mV	This work
MoS ₂ /NiS ₂	1.0 M KOH	278 mV	[7]
Ni-Mo ₂ C/NC	1.0 M KOH	310 mV	[8]
Ni _{0.95} Fe _{0.05}	1.0 M KOH	330 mV	[9]
Ni ₉ S ₈ /MoS ₂ @NiMoO ₄	1.0 M KOH	360 mV	[10]
Cobalt phosphate MFs	1.0 M PBS	457 mV	[11]
Ir _{0.6} Cr _{0.4} O _x -350	0.5 M H ₂ SO ₄	250 mV	[12]
NiFe LDHs	1.0 M K-B _i	360 mV	[13]

Table S10. Comparison of overall water splitting performance of M-NiS/APC with previously reported electrocatalysts.

Catalyst	Electrolyte	Voltage at 10 mA/cm ²	References
NiS/APC	1.0 M KOH	1.56 V	This work
CoMoNiS-NF	1.0 M KOH	1.54 V	[19]
Ni-M@C-130	1.0 M KOH	1.57 V	[14]
WN-Ni@N,P-CNT	1.0 M KOH	1.57 V	[16]
Mo ₂ NiB ₂	1.0 M KOH	1.57 V	[17]
Fe-doped Ni ₃ S ₂	1.0 M KOH	1.58 V	[15]
NF@G-5@Ni ₃ S ₂	1.0 M KOH	1.62 V	[18]
Ni/Mo ₂ C(1:2)-NCNFs	1.0 M KOH	1.64 V	[20]
NMS NFs	1.0 M KOH	1.60 V	[21]

References

- 1 Y. Chen, M. Wang, S. Xiang, J. Liu, S. Feng, C. Wang, N. Zhang, T. Feng, M. Yang, K. Zhang and B. Yang, *ACS Sustainable Chem. Eng.*, 2019, **7**, 10912-10919.
- 2 X. Qiao, H. Kang, Y. Li, K. Cui, X. Jia, H. Liu, W. Qin, M. Pupucevski and G. Wu, *ACS Appl. Mater. Interfaces*, 2020, **12**, 36208-36219.
- 3 Q. Dong, M. Li, M. Sun, F. Si, Q. Gao, X. Cai, Y. Xu, T. Yuan, S. Zhang, F. Peng, Y. Fang, S. Yang, *Small Methods*, 2021, **5**, 2100878.
- 4 E. Vijayakumar, S. Ramakrishnan, C. Sathiskumar, J. Y. Dong, J. Balamurugan, S. Hyun, K. Dawool, Y. H. Kim and H. Lee, *Chem. Eng. J.*, 2022, **428**, 131115.
- 5 C. C. Yang, S. F. Zai, Y. T. Zhou, L. Du and Q. Jiang, *Adv. Funct. Mater.*, 2019, **29**, 1901949.
- 6 A. Munir, T. Haq, M. Saleem, A. Qurashi, S. Z. Hussain, F. Sher, A. Ul-Hamid, A. Jilani and I. Hussain, *Electrochim. Acta*, 2020, **341**, 136032.
- 7 J. Lin, P. Wang, H. Wang, C. Li, X. Si, J. Qi, J. Cao, Z. Zhong, W. Fei and J. Feng, *Adv. Sci.*, 2019, **6**, 1900246.
- 8 B. Wang, F. Shi, Y. Sun, L. Yan, X. Zhang, B. Wang and W. Sun, *Appl. Surf. Sci.*, 2022, **572**, 151480.
- 9 X. Zhang, A. N. Marianov, Y. Jiang, C. Cazorla and D. Chu, *ACS Appl. Nano Mater.*, 2019, **3**, 887-895.
- 10 L. Chen, Z. Deng, Z. Chen and X. Wang, *Adv. Mater. Interfaces*, 2021, **8**, 2101483.
- 11 S. S. Sankar, A. Rathishkumar, K. Geetha and S. Kundu, *Int. J. Hydrogen Energ.*, 2021, **46**, 10366-10376.
- 12 W. Gou, M. Zhang, Y. Zou, X. Zhou and Y. Qu, *ChemCatChem*, 2019, **11**, 6008-6014.
- 13 Y. Dong, S. Komarneni, F. Zhang, N. Wang, M. Terrones, W. Hu and W. Huang, *Appl. Catal. B: Environ.*, 2020, **263**, 118343.
- 14 Y. Yang, H. Yao, Z. Yu, S. M. Islam, H. He, M. Yuan, Y. Yue, K. Xu, W. Hao, G. Sun, H. Li, S. Ma, P. Zapol and M. G. Kanatzidis, *J. Am. Chem. Soc.*, 2019, **141**, 10417-10430.
- 15 K. Srinivas, K. Srinivas, Y. Chen, X. Wang, B. Wang, M. Karpuraranjith, W. Wang, Z. Su, W. Zhang and D. Yang, *ACS Sustainable Chem. Eng.*, 2021, **9**, 1920-1931.
- 16 Q. Zhang, F. Luo, X. Long, X. Yu, K. Qu and Z. Yang, *Appl. Catal. B: Environ.*, 2021, **298**, 120511.
- 17 A. Saad, Y. Gao, K. A. Owusu, W. Liu, Y. Wu, A. Ramiere, H. Guo, P. Tsiakaras and X. Cai, *Small*, 2021, **18**, 2104303.
- 18 D. Lim, E. Oh, C. Lim, S. E. Shim and S. H. Baeck, *Electrochim. Acta*, 2020, **361**, 137080.

- 19 C. Jin, N. Zhou, Y. Wang, X. Li, M. Chen, Y. Dong, Z. Yu, Y. Liang, D. Qu, Y. Dong, Z. Xie and C. Zhang, *J. Electroanal. Chem.*, 2020, **858**, 113795.
- 20 M. Li, Y. Zhu, H. Wang, C. Wang, N. Pinna and X. Lu, *Adv. Energy Mater.*, 2019, **9**, 1803185.
- 21 Y. Qian, J. Yu, Y. Zhang, F. Zhang, Y. Kang, C. Su, H. Shi, D. J. Kang and H. Pang, *Small Methods*, 2021, **6**, 2101186.